Fermilab-Pub-12-581-APC October 2012

Proposed triple-wall, voltage-isolating electrodes for multiple-bias-voltage 3D sensors*

Sherwood Parker[a], N.V. Mokhov[b], I.L. Rakhno[b], I.S. Tropin[b], Cinzia DaVia[c], S. Seidel[d], M. Hoeferkamp[d], J. Metcalfe[d], Rui Wang[d], Christopher Kenney[e], Jasmine Hasi[e], Philippe Grenier[e]

[a]*University of Hawaii, Honolulu, HI 96822, USA*
[b]*Fermilab, P.O. Box 500, Batavia, IL 60510, USA*
[c]*The University of Manchester, Particle Physics Group, Oxford Road, M139PL Manchester, UK*
[d]*University of New Mexico, Department of Physics and Astronomy, 1919 Lomas Blvd NE, Albuquerque, NM 87131-0001, USA*
[e]*SLAC National Accelerator Laboratory, 2575 Sand Hill Road, Menlo Park, CA 94025-7015, USA*

October 25, 2012

Abstract

Dividing 3D active-edge silicon sensors into separate sections with a triple-wall sandwich of two trench electrodes separated by an insulating layer, will allow two or more bias voltages to be used simultaneously. Such sensors could be fabricated with only a single group of low-temperature additional steps and may be necessary to prevent a new form of radiation-damage failure in non-uniform radiation fields.

*This work was supported by the UK-STFC, the U.S. Department of Energy including grants to the University of Hawaii, Grant no. DE-FG02-04ER41291, Fermi Research Alliance, LLC contract DE-AC02-07CH11359, Univ. of New Mexico award DE-AC02-98CH10886, number 95247.

1. A new radiation damage problem

The required bias voltage for full depletion and maximum signal [1] and the breakdown voltage [2, 3] both increase as silicon sensors are irradiated, the later from the extra voltage drop in the irradiated substrate. Table 1 shows these voltages for ATLAS sensors with 3-signal-electrodes in each 50 μm × 400 μm pixel with 0, 2×10^{15}, 5×10^{15}, 1×10^{16}, and 2×10^{16} 800 MeV protons/cm^2 [4].

In colliding beam machines, important information can be found using a subset of events in which the incoming protons remain intact and scatter at small angles [5, 6]. Having lower momenta, they can be bent out of the beam envelope and detected with silicon sensors placed close to the circulating beams.

The closer the sensors can be placed to the beam, the larger the kinematic range that can be covered, with 2 – 3 mm a goal for the 220 m proposals [5, 6]. The edge closest to the beam will receive the heaviest irradiation. Proton-proton collisions dominate significantly even at the TOTEM luminosity of 10^{33} cm^{-2}s^{-1}. Backgrounds induced by tails from the collimators and beam-gas elastic and inelastic scattering are of the order of 0.1-1% of the total rates at the TOTEM Roman pots [7].

For heavily irradiated sensors, the depletion voltage and the bias voltage to get an optimum signal are above the breakdown voltages of un-irradiated sensors. The larger values of the bias voltage for optimum signal size is due to the fact that not all the charge is collected even from fully depleted sensors due to charge carrier capture at damage sites.

2. Sensor Measurements

The signal and leakage currents are measured with the apparatus shown in Figure 1. The measurements started with the sensors at +20º C and for the un-irradiated sensor, low humidity (17% which is in the normal range for heated rooms in the New Mexico desert), followed with N_2.substitution, then temperature reduction.

The increase in signal amplitudes as the bias voltage is increased beyond the full depletion voltage can be seen in Figure 2 which shows signal amplitudes from the sensors for four levels of irradiation, and with both the signal and leakage currents extended into the breakdown region. Beyond the usual increase of leakage currents with temperature, the insensitivity of these measurements to temperature, and over a limited range, to humidity is also shown.

The amount and location of possible surface charges were not measured. They are known to affect the behavior of silicon sensors [8, 9] and the difference between the SLAC (63V) and New Mexico (109V) values of breakdown voltages suggest they may play a significant role. There are field lines between N and P electrodes that loop outside the sensor. Charges can drift along them until they reach the oxide surface, and then move along it until the field parallel to the surface is zero. Additional following charges from the same region, repelled by the first, would not go as far, eventually tending to make an equipotential surface region that would have opposite-sign surface charges grouped near each electrode. This would increase the fields around the electrodes and could affect the breakdown voltages.

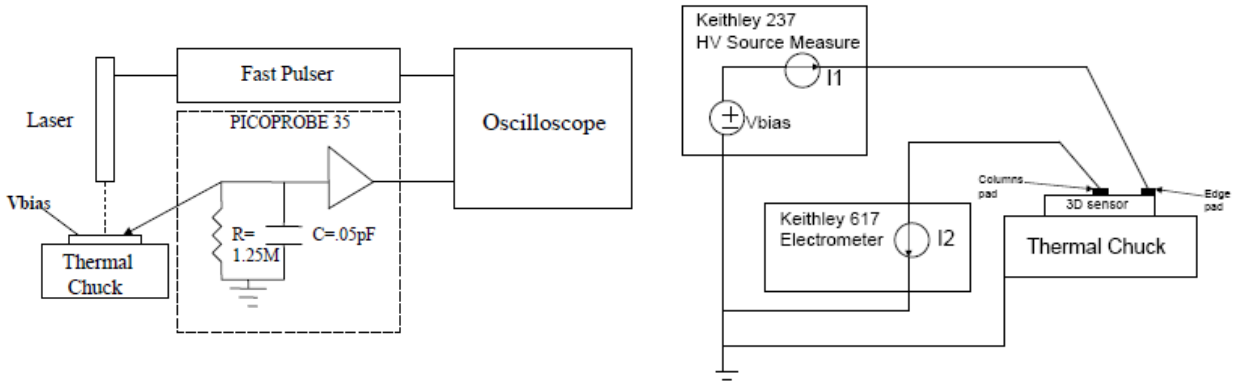

Fig. 1 U. of New Mexico apparatus to measure signal charge as a function of irradiation level and bias voltage (left) and leakage currents I2 (right).

Laser: 1064 nm EG&G, **Probes**: Picoprobe 35 26 GHz, Cascade Microtech coaxial
Oscilloscope: Tektronix TDS7254 2.5 GHz, **Thermal Chuck:** Micromanipulator (-60º C)

It should be noted that ATLAS radiation-tolerance measurements have generally been done with detectors that are first irradiated, stored while induced radiation dies down, and then measured in a low-intensity beam. In reality the high track rate will generate large amounts of charge in any kind of gas at any temperature with support structure details being important. Regardless of this factor, both the need for and tolerance of higher bias voltages with irradiation are clear.

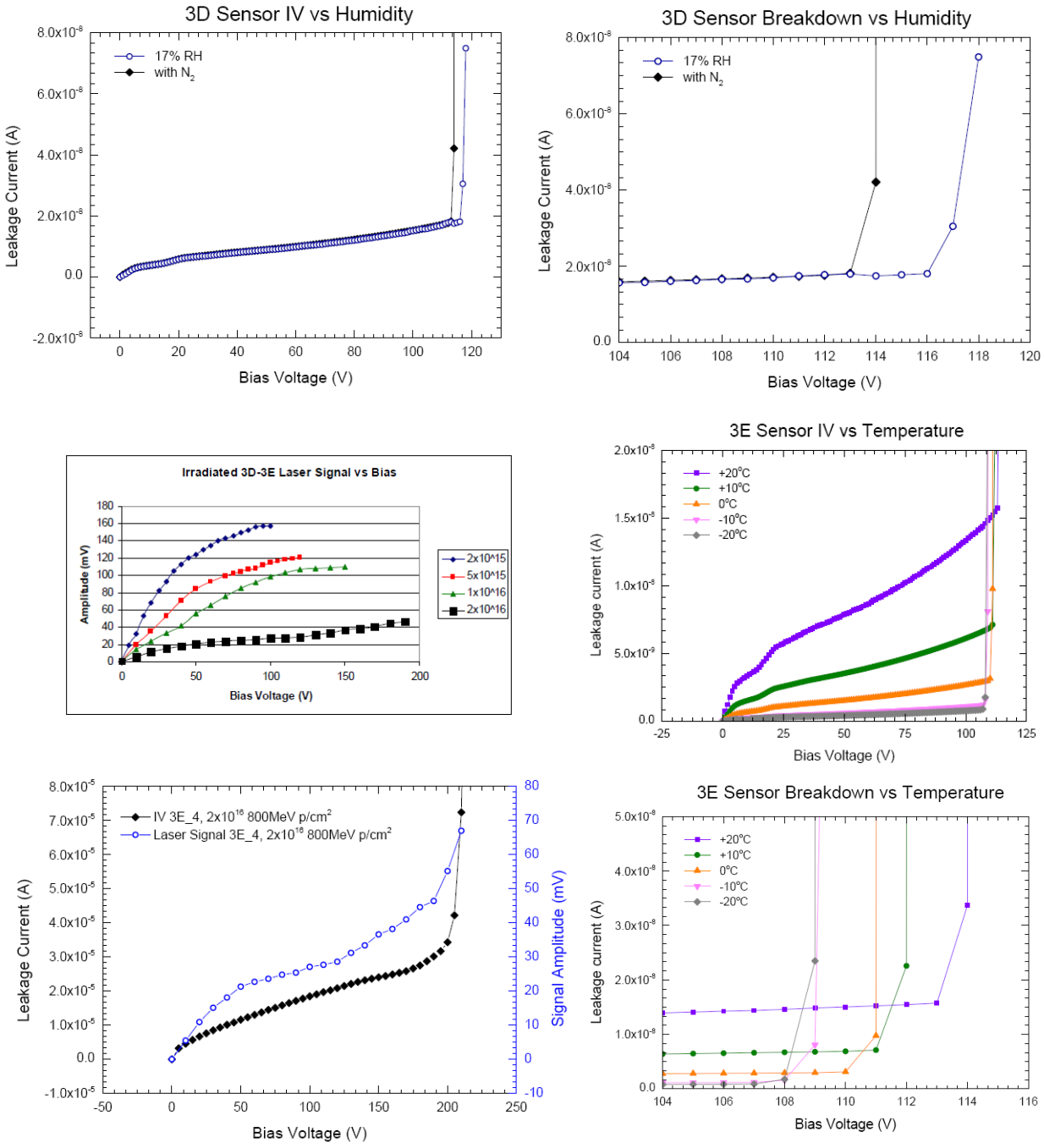

Fig. 2. Signals and leakage currents from 3D sensors with three electrodes per 50 µm × 400 µm pixel. (clockwise from top left) (1) effect of humidity on breakdown bias voltage: 20° C, lab air vs. nitrogen, (2) expanded voltage scale, (3) effect of temperature, (4) temperature, expanded voltage scale, (5) signal and leakage currents after irradiation by 2 × 10^{16} / cm^2 800 MeV protons, (6) signal currents for four irradiation levels down to 2 × 10^{15} 800 MeV protons showing both the need and tolerance of higher bias voltages. The decreased signal and the slope over the bias voltage range are due to both charge carrier capture and depletion voltage increase. (1) – (4) are for a small, un-irradiated test sensor, (5) and (6) are for full size ones.

sensor	irradiation level		irradiated V_{bias} from		$V_{breakdown}$	
	800 MeV protons	1 MeV eq. neutrons.	signal	CV	un-irrad.	irrad.
0	0	0	---	---	63, 109 V	---
3	2×10^{15} cm^{-2}	1.42×10^{15} cm^{-2}	90 V	75 V	---	90 V
1	5×10^{15} cm^{-2}	3.55×10^{15} cm^{-2}	110 V	100 V	68 V *	170 V
5	1×10^{16} cm^{-2}	7.10×10^{15} cm^{-2}	120 V	115 V	65 V *	190 V
4	2×10^{16} cm^{-2}	1.42×10^{16} cm^{-2}	180 V	145 V	71 V *	215 V

Table 1: Bias voltages for full depletion, maximum charge collection from full volume, and breakdown voltages for sensors with three signal electrodes in each 50 μm × 400 μm pixel. Un-irradiated sensor 0 (a small test chip with fewer pixels) and all irradiated sensors are measured at -20° C. * Un-irradiated sensors 1, 4, and 5 are measured at + 20°. Breakdown voltage of sensor 0, measured at + 20° at SLAC prior to shipment to New Mexico was 63 V.

Item	RP1	RP2	RP3	RP4	RP4h
Distance from IP (m)	140	147	180	215	215.3
Orientation	V	V	V	V	H
Charged hadrons	7.5	2.9	1.0	0.58	6.7
Neutrons	3.7	1.3	0.61	0.37	1.4
Electrons	115	28	23	12	18
Photons	1410	279	187	81	147
D_{max}	12	10	20	1.9	55
D_{av}	3.4	1.1	0.69	0.37	1.2
d_{si}	10.36	10.33	8.77	5.97	2.10

Table 2: Total particle fluxes (10^5cm^{-2}s^{-1}) averaged over silicon sensors, peak D_{max} and average D_{av} absorbed doses (in units of 10^4 Gy/yr) at a luminosity of 10^{33} cm^{-2}sec^{-1}, and the approach distance, d_{si} (mm) [7]. The orientation indicates whether the silicon sensors are above and below the beam (V) or horizontally away from it (H).

3. Beam calculations

The expected variation of irradiation levels with position has been calculated with the MARS Monte-Carlo code [10] for 220 m from the IP5 (CMS) [7] interaction point and the calculations for the IP1 (ATLAS) 220m forward proton proposal are underway. Figure 3 shows the neutron and charged hadron flux (cm^{-2}s^{-1}) as a function of position at a luminosity of 10^{33} cm^{-2}s^{-1} calculated for Roman pot 4h, the last of the

Roman pots. The horizontal separation from the beam center line from the inner edge of the silicon sensor is comparable to the 2 – 3 mm planned for ATLAS AFP. It can be seen that the charged particle flux varies by a factor of over 100 within 5 mm. If the LHC ran for 2/3 of the time at 10^{34} $cm^{-2}s^{-1}$, the maximum-flux square in the plot would get 6.3 x 10^{15} tracks cm^{-2} per year. Table 2 shows the approach distances, d_{si} and the maximum dose, D_{max}, which multiplying by 10 for the higher ATLAS and CMS luminosity ranges, for the 5 Roman pots, from 7 x 10^{14} to 2 x 10^{16} tracks cm^{-2} per year.

4. Readout solution, consequences

The proposed solution for a pixel readout chip that can handle the expected intense radiation levels is to use the FEI4 which is fabricated in 130 nm technology with a very thin gate oxide. It works even after 200 MRad [11, 12]. Its large size, with a pixel input area of 16.8 mm x 20 mm also covers the area in which the scattered protons are expected to be found. But that large size means the pixel sensor, using a bias voltage that provides adequate efficiency in the most heavily irradiated part will cause breakdown in the least irradiated parts.

Simultaneously bump-bonding separate smaller sensors, each run at a different bias voltage, to the FEI4, is somewhere between difficult and completely impractical when the actual shapes of the heavily and lightly irradiated areas in Fig. 3 are considered.

3D sensors [3] are generally useful for forward physics applications as they have the greatest resistance to radiation damage of any type of silicon sensor [13 – 14], with lower depletion voltages, less charge capture, less heating, as they not require bias voltages of 1,000V or more, and after the extreme irradiation expected, would still have double the signal of planar sensors. In addition, they can be made with active-edges which are efficient to within a micron of the sensor physical edges rather than hundreds of microns [16]. Even so, 3D sensors could be subject to the problem that an adequate bias voltage for one part would cause breakdown in other parts. One method, the use of smaller 3D inter-electrode separation in heavily irradiated regions is possible and can be incorporated without extra fabrication steps, but is inflexible and before irradiation might have the simultaneously-too-high / too-low bias voltage problem.

So if the track intensity and non-uniformity are as large downstream from ATLAS as the calculations indicate they are for CMS, both forward ATLAS and possible CMS sensors – even radiation-hard 3D ones – will face a serious problem.

5. Possible sensor solution

This note describes a new form of 3D sensor that can solve this simultaneously-too-high / too-low bias voltage problem.

Figure 4 shows a schematic view of part of an active-edge, 3D sensor that will allow the simultaneous use of two or more adjustable bias voltages by replacing one or more selected rows of p^+ bias electrodes with two inner active-edges separated by insulating sections to isolate the different voltages.

Once the support wafer is removed, the resulting sensor will be mechanically fragile. To guard against breakage it would be possible to bond the sensor to a thin, low-atomic-number permanent support plate made out of boron carbide or similar material. (The coefficient of thermal expansion of boron carbide is double that of silicon, which may limit the thickness used.)

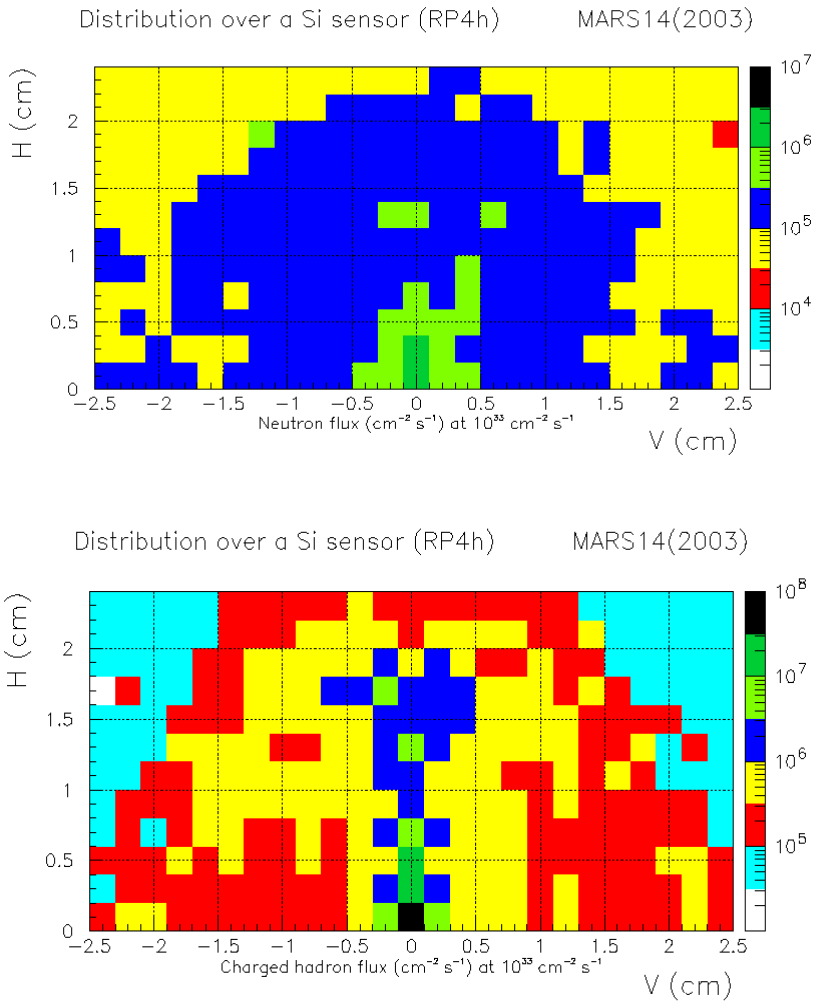

Fig. 3. Calculated flux ($cm^{-2}s^{-1}$) of neutrons and charged hadrons as a function of position at a luminosity of 10^{33} $cm^{-2}s^{-1}$ for the TOTEM detector RP4h. The horizontal and vertical axes are labelled with H and V, respectively. The beam center line in the plot is below the center of the bottom of the plot. The horizontal separation in actual space is 2.1 mm.

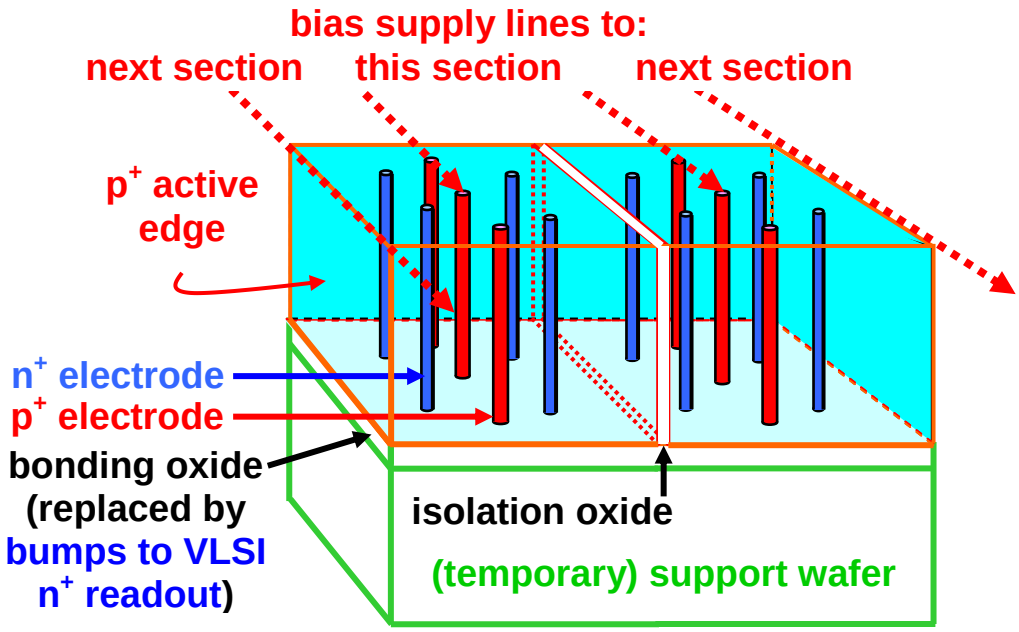

Fig. 4. Schematic view of part of a 3D sensor with two halves separated by their two active edges and an insulating section. Readout and bias supply sides can be switched.

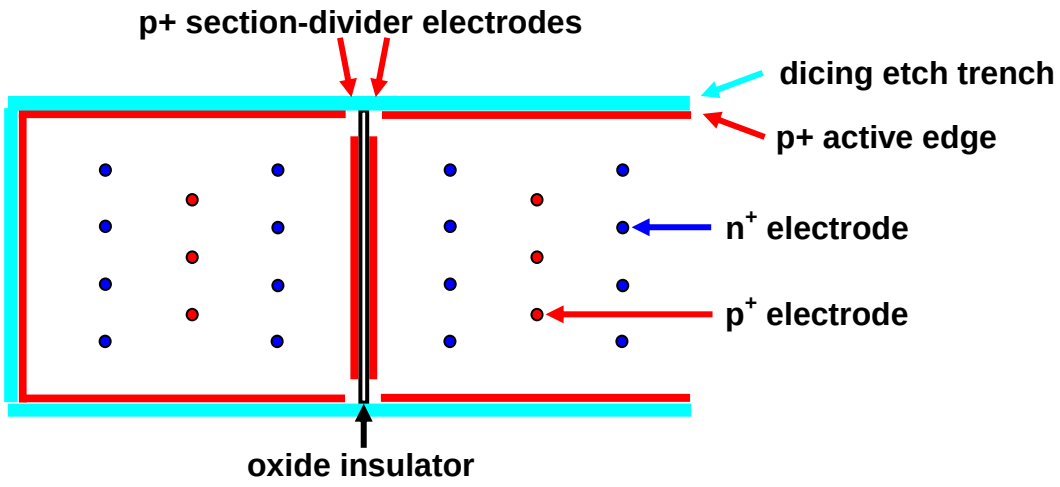

Fig. 5. Simplified schematic view of deep-reactive-ion etching regions for a multiple-bias-voltage 3D sensor.

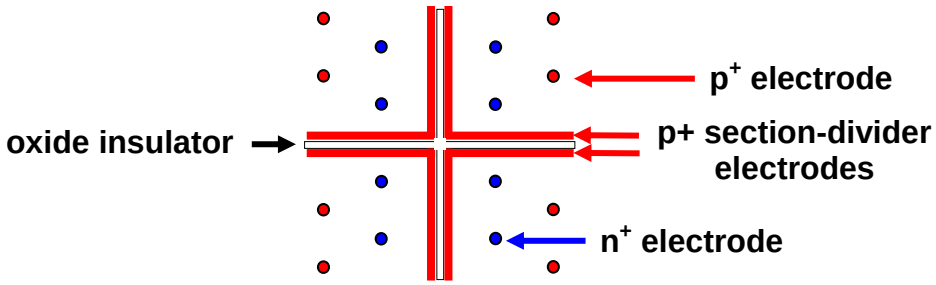

Fig. 6. Simplified schematic view of the region around a junction of four bias voltage regions separated by triple-wall voltage isolators.

The trenches could be curved to correspond to the expected two-dimensional radiation dose functional form. However this could require a different design for each location. A better design would use a regular 2-dimensional array of such triple-wall electrodes. Separate conductors running in from the sensor edges could provide a bias voltage for each section which would have all bias electrodes of each section electrically connected. Usually two contacts are used for redundancy. In the forward proton 220 m detector there are always one or more free sides, allowing the sensor to extend beyond the readout chip where connections can be made to the bias electrode metal lines. One can also form the bias contacts by wire bonding to the side away from the readout chip which is exposed and available for bias voltage contacts once the oxide is removed at one or more bias electrodes.

One can plasma dice the final sensor into multiple die, even with non-Cartesian shapes. This avoids mechanical breakage concerns, but would necessitate additional bump bonding steps.

6. Fabrication steps

Although not strictly required, the fabrication steps for the isolation section divider can follow the fabrication of the n^+ and p^+ column electrodes. The p^+ section-dividing electrodes and the p^+ active-edges would be made at the same time, and with some care in the etching step, all p^+ electrodes could be made at the same time.

The fabrication steps would be:

6.1 formation of the oxide and nitride passivation / diffusion barrier layers.

6.2 p-spray implants, reaching inside the surface field oxide layers (to prevent the positive oxide interface charge from attracting a layer of mobile electrons that would short together the n^+ signal electrodes).

6.3 oxide-bonding of the device wafer to a support wafer. (Oxidized facing surfaces of both wafers are coated with a liquid such as H_2O_2 or NH_4OH which forms hydrogen bonds that causes clean wafers to snap together. Heating drives out H_2O and leaves the wafers bonded with strong, high-temperature Si-O-Si bonds.)

6.4 n-electrode deep reactive ion etch, doping / filling with polycrystalline silicon {poly), drive-in.

6.5 p-electrode deep reactive ion etch, doping / filling with poly, and drive-in.

6.6 active-edge and dividing-electrode etch, filling with poly, doping, drive-in, and CMP. (CMP – chemical-mechanical-planarization – is an industry standard

process normally used for making multiple levels of metal and which can be used to thin wafers.) CMP would be used as needed following trench-filling steps 6 and 7 to remove the ridge of filling material which could interfere with the needed uniform application of photo resist for the following step. (Ridges of the same height but smaller in lateral extent around column electrodes do not interfere as much with photo-resist applications.)

6.7 The only extra group of steps – lithography, trench etch, oxide deposition, CMP – for the formation of the oxide insulator, would come here.

6.8 Metal and scratch mask steps would follow.

Steps 6.4 – 6.7 would use the bonding oxide to the support wafer for the deep reactive ion etch-stop. In step 7, the p-spray layers would be removed as part of the trench etching, providing electrical isolation between adjacent sections. The trench etch in step 6 goes more rapidly than that of the electrode holes in step 5, but if the two are done separately, require separate poly depositions so the second photo-resist does not have to cover a deep hole. Since the poly comes out on the tube wall and eventually requires laborious cleaning, combining the steps does help.

Figure 5 shows a schematic layout, with the FEI4-column direction horizontal, for items 4 – 7. Only 4 rather than 80 columns are shown and the distance from the left edge, which is closest to the beam, to the (first) section divider would normally be larger.

The gaps in the active-edge electrodes around the section divider are to prevent edge sections from being shorted by the boron dopant which will be diffused out from the deposited active edge electrodes during the drive-in. The gaps would not be needed for bias voltage sections away from any edges as shown in Figure 6. In principle, if the dicing etch could remove all silicon beyond the ends of the oxide insulator, the gaps would not be necessary. This would not involve a difficult alignment job if the insulator projected far enough into the dicing etch region, but the further it does, the less uniform the sensor edge since the silicon etch would not remove the oxide. For isolated-chip applications such as the planned ATLAS forward proton detector at 220 m, the projection would not be a problem and continuous active-edge electrodes might be used.

For this use, the leftmost pixels in Figure 4 will probably be lengthened so the sensor reliably extends beyond the FEI4 readout chip which may have a border up to 100 microns beyond the last bump-bonds plus a dicing saw safety margin of some tens of microns.

7. Filling the insulating trench

The oxide trench would be etched just like the others, but the filling steps would differ. No top-side nitride diffusion barrier would be needed.

TEOS (tetraethooxy silane), deposited by plasma-enhanced chemical vapor deposition to form SiO_2, makes one of the most conformal films, and so would easily fill the trench as long as the walls are parallel [17]. While the quality of the film is not as high as that of a thermal oxide, the substantial trench width makes a layer that would easily withstand typical bias voltages let alone bias voltage differences. Water absorption would be prevented by the standard low temperature oxide scratch mask which is deposited on top at a later step.

There are several other methods that might be used. In all cases, a conformal insulating layer is needed with its minimum thickness set by the required dielectric strength.

A thermal oxide might be grown in the trench to start, but with the present deep reactive ion etching machines having 30 to 60 to 1 depth-to-width ratios, the minimum trench widths are in the 4 to 8 micron-range, and a 2 to 4 micron thermal oxide would take rather long to grow.

Narrowing the trench with the preliminary deposition of a conformal polycrystalline silicon layer would short out the two sides with a conductive bottom layer, but this bottom layer could be removed by a short anisotropic etch, while leaving the poly on the sidewalls. A trench-filling poly layer could also be deposited after the initial insulating dielectric, so avoiding an electrical short between the sensor subsections. Making a single wide poly divider in step 6, which is then etched out in step 7, rather than two narrower poly-filled trenches, results in more poly to be cleaned off the tube walls and so is not desirable.

Alternatively, atomic-layer deposition could be employed to deposit any of a variety of highly conformal passivating dielectrics.

8. Additional item

As with the polycrystalline silicon deposition, the boat for the oxide deposition should have wide enough wafer holding grooves so the wafers can tilt slightly with only a three-point contact with the boat. The wafers will also need to be rotated periodically so they are not glued to the boat by the deposited poly and oxide.

9. Conclusions

Any forward CMS sensors at 220 m operating at the planned LHC luminosities will face a serious problem from a new form of radiation-damage failure due to the highly non-uniform radiation fields close to the beam where they must operate. The needed bias voltages in the heavily irradiated regions will be above breakdown levels in lightly irradiated ones nearby. The planned forward ATLAS sensors – even radiation-hard 3D ones – will face a similar problem if the track intensity and non-uniformity are as large 220 m from the ATLAS intersection region as calculations indicate they are for CMS. The addition of interior triple-wall electrodes having a central insulating trench between two electrodes similar to those in a 3D active edge silicon sensor, will allow two or more bias voltages to be used simultaneously. Such sensors could be fabricated with only a single group of low-temperature additional steps.

References

[1] E. Heijne, “Muon flux measurement with silicon detectors in the CERN neutrino beams”, CERN 83-06, p. 111.

[2] V. Eremin, E. Verbitskaya, Z.Li, A. Sidorov, E. Fretwurst, G. Lindstrom, “Scanning transient current study of the I-V stabilization phenomena in silicon detectors irradiated by fast neutrons”, *Nucl. Instr. and Meth. A* **466** (2001) 308.

[3] S. I. Parker, C. J. Kenney, and J. Segal, “3D--A proposed new architecture for solid-state radiation detectors”, *Nucl. Instr. and Meth*, **A395** (1997) 328-343. (See Figure 5.)

[4] M. Hoeferkamp, “ATLAS 3D Sensor Proton Irradiations”, LBNL ATLAS Upgrade Workshop, 22 May 2008.

[5] M. G. Albrow, et al., “The FP420 R&D Project: Higgs and New Physics with forward protons at the LHC”, arXiv:0806.0302v2 [hep-ex] 2 Jan 2009.

[6] L. Adamczyk, et al., “AFP: A Proposal to Install Proton Detectors at 220m around ATLAS to Complement the ATLAS High Luminosity Physics Program”, May 5, 2011,http://www-

hep.uta.edu/~brandta/ATLAS/AFP/TP-report-May52011.pdf

[7] N.V. Mokhov, A.I. Drozhdin, I.L. Rakhno, D. Macina, "Accelerator related backgrounds in the LHC forward detectors", in *Proc. of 2003 Particle Accelerator Conference*, **Conf.Proc. C030512 (2003) 1742.**

[8] A. Longoni, M. Sampietro,L. Strüder, "Instability of the behavior of high resistivity silicon detectors due to the presence of oxide charges", *Nucl. Instr. and Meth.* A**288** (1990) 35.

[9] A. Chilingarov, D. Campbell, G. Hughes "Interstrip capacitance stabilization at low humidity" *Nucl. Instr. and Meth.* A **560** (2006) 118–121.

[10] N.V. Mokhov, "The Mars Code System User's Guide", Fermilab-FN-628 (1995); N.V. Mokhov, S.I. Striganov, "MARS15 Overview", in *Proc. of Hadronic Shower Simulation Workshop*, Fermilab, Sept. 2006, AIP Conf. Proc. 896, pp. 50-60 (2007); http://www-ap.fnal.gov/MARS/.

[11] M. Garcia-Sciveres, et al., "The FE-I4 pixel readout integrated circuit", *Nucl. Instr. and Meth. A* **636** (2011) S155–S159.

[12] Marlon Barbero, et al., "Submission of the first full scale prototype chip for upgraded ATLAS pixel detector at LHC, FE-I4A", *Nucl. Instr. and Meth. A* **650** (2011) 11

[13] S. Parker and C. Kenney, "Performance of 3-D Architecture Silicon Sensors After Intense Proton Irradiation", *IEEE Trans. Nucl. Sci*. **48** (2001) 1629.

[14] C. Da Via´, J. Hasi, C. Kenney, V. Linhart, Sherwood Parker, T. Slavicek, S.J. Watts, P. Bem, T. Horazdovsky, S. Pospisil, "Radiation hardness properties of full-3D active edge silicon sensors", *Nucl. Instr. Meth. A* **587** (2008) 243–249.

[15] C. Da Viá, E. Bolle, K. Einsweiler, M. Garcia-Sciveres, J. Hasi, C. Kenney, V. Linhart, Sherwood Parker, S. Pospisil, O. Rohne, T. Slavicek, S. Watts, N. Wermes, "3D active edge silicon sensors with different electrode configurations: Radiation hardness and noise performance", *Nucl. Instr. Meth A* **604** (2009) 505.

.[16] Cinzia Da Già, Mario Deile, Jasmine Hasi, Christopher Kenney, Angela Kok, Sherwood Parker, Stephen Watts, et al., "3D Active Edge Silicon Detector Tests with 120 GeV Muons", *IEEE Trans. Nucl. Sci.* **56** (2009) 505.

[17] J. Plummer, M. Deal, P. Griffin, "Silicon VLSI Technology", (2000) pp, 710, 718, Prentice Hall, Upper Saddle River, NJ 07458.